Simulation of Hydrostatic Pockets Between the Cylinder Block and Valve Plate of a Piston-type Pump

Haotian Han[1], Thomas Heeger[2], Lizhi Shang[1], and Liselott Ericson[2]

[1]Maha Fluid Power Research Center, Purdue University, West Lafayette, Indiana, USA
[1]E-mail: han592@purdue.edu; shangl@purdue.edu
[2]Fluid and Mechatronic Systems, Linköping University, Linköping, Sweden
[2]E-mail: thomas.heeger@liu.se; liselott.ericson@liu.se

Abstract

Piston-type positive displacement machines are used across diverse applications and operating conditions, making it a critical design challenge to balance the minimization of solid-body contact while maintaining efficiency. This study investigates the potential of hydrostatic pockets between the cylinder block and valve plate to provide dynamically and passively controlled pressure forces, mitigating contact issues at low speeds without excessive losses at high speeds.

Simulations of a baseline pump design revealed persistent solid-body contact under low-speed and high-pressure conditions, indicating the need for enhanced lubrication strategies. Retaining the baseline design, the study examined multiple hydrostatic pocket configurations through simulation, varying their location and quantity. Although the primary focus is on low-speed high-pressure and high-speed high-pressure scenarios, additional operating points at high-speed low-pressure and medium-speed medium-pressure were also considered.

The effectiveness of each design was evaluated on the basis of film thickness, contact pressure, and viscous losses under key operating conditions. The experimental findings from previous studies were used to validate or challenge the conclusions from the simulation results. This paper seeks to deliver a better understanding of the hydrostatic pockets, offering design guidance for optimizing the lubrication management for future piston-type positive displacement machines and informing strategies for improved efficiency and longevity in demanding applications.

Keywords: contact, cylinder block, efficiency, hydrostatic, lubrication, piston-type pump, simulation, valve plate

1 Introduction

Piston-type positive displacement machines are used in various industries, including off-highway vehicles, aviation, automotive, etc. due to their high efficiency and strong reliability over a wide range of operating conditions [1]. However, with the modern trend toward electrification, these machines must now adapt to an even wider range of operating conditions. This expansion has revealed limitations in current axial piston machines, particularly their inability to operate efficiently and reliably at extremely low and high speeds [2].

To combat these challenges, Ericson and Forssell proposed the Floating Piston pumps [3] as shown in Figure 1. This innovative design minimizes the centripetal force acting on the cylinder block, which enables this pump to operate at higher speeds without causing cylinder block unbalance.

Among the three primary lubricating interfaces in Floating Piston pumps: swash-plate/piston-plate, piston-ring/cylinder-bore, and cylinder-block/valve-plate; since the piston plate does not carry radial forces and the friction losses at the piston-ring/cylinder-bore interface are minimal [3], the cylinder-block/valve-plate interface is the most complex [4, 5]. This complexity arises because it must balance the axial force from the displacement chambers and the tilting moment generated by the radial force based on the crowning point location; therefore, the cylinder-block/valve-plate interface requires detailed design to maintain high performance.

At higher rotational speeds, the relative sliding motion between the stationary valve plate and the rotating cylinder block generates hydrodynamic effects within the fluid lubricating interface [6]. These effects lift the cylinder block from the valve plate, reducing solid-body contact. Additionally, the hydrodynamic effects help balance the net moment acting on the cylinder block, reducing tilting and the risk of metal-to-metal contact [4].

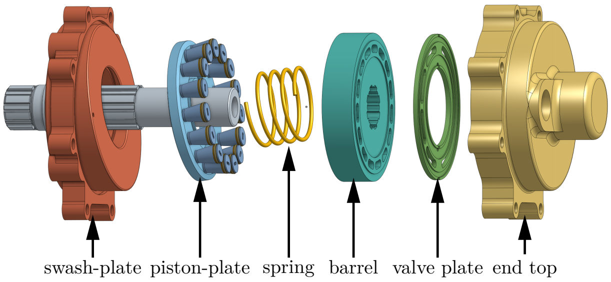

Figure 1: Floating Piston Pump Components [3]

However, at low speeds, the hydrodynamic effects diminish drastically, which leaves the cylinder block under-supported, causing solid-body contact and damage [4]. Moreover, this damage further reduces the lubricating interface's ability to generate hydrodynamic forces and increases leakage, compromising the machine's performance. To address this issue, Achten et al. introduced a novel hydrostatic bearing within the cylinder block sealing land of a floating cup pump [7]. Experimental validation by Achten et al. demonstrated the ability of this design to provide hydrostatic support to the cylinder block, particularly at extremely low speeds when hydrodynamic forces are insufficient, while also improving efficiency [2].

This study uses numerical simulations to explore the working principles and evaluate the effectiveness of hydrostatic pockets between the cylinder block and valve plate in a Floating Piston pump. The focus is on comparing contact severity, power loss, and gap height distribution under low-speed high-pressure and high-speed high-pressure conditions; additionally, the study evaluates performance at other operating points, including high-speed low-pressure and medium-speed medium-pressure conditions. While the study is performed using a Floating Piston pump platform, the findings are applicable to all piston-type hydraulic machines. The findings seek to provide a deeper understanding of the potential of hydrostatic pockets, contributing to the optimization of piston-type positive displacement machines for a wider range of operating conditions.

2 Related Literature

This section summarizes literature on Floating Piston pump working principles and the design of the cylinder-block/valve-plate lubricating interface.

2.1 Floating Piston Pump Design

The design of a Floating Piston pump is based on the swashplate-type axial piston pump, where the cylinder block, valve plate, and port block are positioned perpendicular to the drive shaft; however, it incorporates several key design differences. As shown in Figure 1, the Floating Piston pump eliminates slippers, fixing the pistons directly onto an inclined plate, known as the piston plate. Ericson and Forssell have explained the working principles and benefits of this novel piston machine [3].

With the piston heads and sealing rings fixed perpendicularly to the piston plate, displacement chamber pressure forces are directly transferred to the pistons and balanced by the piston-plate/swash-plate lubricating interface. This design prevents side forces on the cylinder block. However, the tilted pistons create a wedged volume in the cylinder bore shown in Figure 2a. The pressurized fluid creates a force imbalance within the displacement chamber, generating a radial force that acts perpendicular to the cylinder bore and on the cylinder block. With a properly positioned cylinder-block/shaft reaction point, the moment generated by this radial force on the cylinder block remains symmetric throughout a revolution and can be balanced [3].

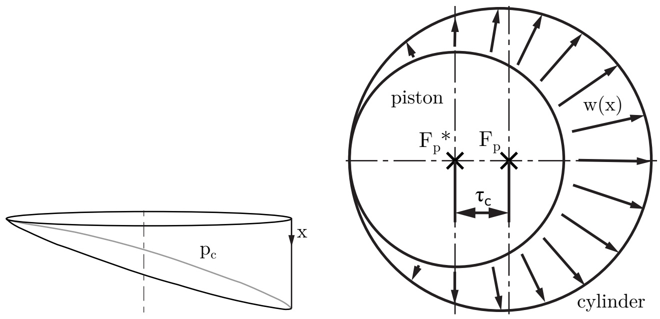

(a) The wedge volume *(b) Force per unit of one piston*

Figure 2: The Pressurized Volume in a Piston Chamber [3]

Moreover, in traditional axial piston machines, the mass of the piston-slipper assembly, as well as the fluid volume, generates centrifugal forces that the cylinder block must balance. These forces create a moment and introduce additional tipping motivation to the cylinder block. Since these forces are proportional to the square of the shaft speed, traditional machines are highly sensitive to rotational speed, creating a barrier to achieving higher operating speeds. In contrast, the Floating Piston pump connects the pistons on a piston plate, balancing their centrifugal forces and eliminating centrifugal forces transmitted from the piston plate to the cylinder block. Additionally, due to the small dead volume and low piston strokes, the centrifugal forces and moments generated by the fluid volume are also minimized [3]. As a result, this optimized design is expected to enable much higher rotational speeds without requiring an overpowering hold-down central spring, which could otherwise cause additional power losses.

2.2 Block Sealing Land Design

The cylinder-block/valve-plate lubricating interface is one of the most critical design aspects of piston-type positive displacement machines. This interface bears the responsibility of providing pressure forces to lift the cylinder block away from the valve plate, sealing high-pressure fluid to prevent leakage into the casing, and balancing moments acting on the cylinder block. These functions are achieved through the thrust effect of rapid gap height changes and the wedge effect resulting from converging and diverging surfaces in the circumferential direction. The gap height of the cylinder-block/valve-plate lubricating interface is determined by various factors, including moment and force balances, which are coupled with solid-body deformation. Ultimately, the gap height influences the elasto-hydrodynamic effects, which directly impact power losses in this interface through viscous dissipation, volumetric losses, and solid-body contact friction.

2.2.1 Hydrostatic Compensation Ratio

Traditionally, an analytical starting point of the block sealing land design is based on the compensation ratio ζ, which compares the loading forces F_{load} and the compensating hydrostatic forces F_{comp}, see Eq. 1 and Figure 3.

$$\zeta =: \frac{F_{\text{load}}}{F_{\text{comp}}} \tag{1}$$

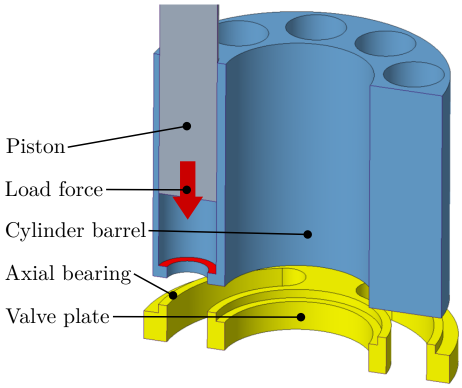

Figure 3: Load Force and Axial Bearing Between the Valve Plate and Cylinder Block [8].

The compensation ratio only considers hydrostatic forces. The load originates from the pressurized chambers pushing the cylinder block against the valve plate, and the compensation force is defined by the area of the hydrostatic bearing [1].

Compensation ratios above 100 % lift the cylinder block off the valve plate, causing undesired leakage from the high-pressure port. Thus, compensation ratios need to be smaller than 100 %. On the other hand, solid contact between the valve plate and cylinder barrel causes wear. The combination of the two requirements leads to compensation ratios just below 100 % [1, 8, 9]. However, note that there are different calculation methods for the compensation ratio [8], and Ernst and Vacca [5] claimed that the hydrodynamic forces in pumps are drastically underestimated, with Vacca and Franzoni [10] stating that typical hydrodynamic forces are in the range of 10 to 20 % of the load forces.

2.2.2 Hydrodynamic Effects

In a traditional cylinder-block/valve-plate sealing land design, the fluid forces in the lubricating interface depend not only on the pressure from the inlet, outlet ports as well as the casing, but also, more importantly, on the elasto-hydrodynamic wedge and squeeze effects between the valve plate and cylinder block surfaces [5, 11]. However, generating pressure from the wedge effect requires sufficient relative sliding velocity between the two opposing surfaces; consequently, at low speeds, the cylinder-block/valve-plate lubricating interface loses its ability to create effective hydrodynamic wedge pressure, often resulting in metal-to-metal contact.

2.2.3 Design with Hydrostatic Pockets

In 2010, Innas introduced a new feature within the lubricating interface incorporating additional chambers in the sealing land, called hydrostatic pockets, along with grooves that connect these pockets to the displacement chamber [7] as shown in Figure 4.

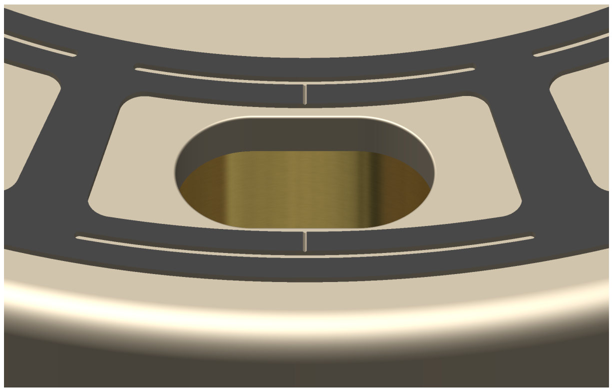

Figure 4: Cylinder Block with Pockets

The pressure in these hydrostatic pockets is determined by multiple flow paths. First, the grooves between the displacement chamber and the hydrostatic pockets act as constant orifices. As the displacement chamber pressurizes, hydraulic oil flows into the pocket and pressurizes it. Simultaneously, the sealing lands between the pocket and the displacement chamber as well as between the pocket and the casing act as variable orifices. These variable orifices are passively controlled by the lubricating film gap height distribution [2] as shown in Figure 5 below.

This design provides several benefits, as suggested by Achten et al. [2]. First, the hydrostatic pockets provide additional pressure forces to support the cylinder block to prevent contact with the valve plate even at extremely low shaft speeds, which leads to the diminishing of contact power losses and surface damage. Additionally, the hydrostatic pockets can dynamically balance the cylinder block; when the cylinder block is tilted, the local gap height becomes extremely small, causing the variable orifices' areas connecting the pockets in the outer edge of the sealing land and the casing to reduce to nearly zero. This effectively cuts off the outlet flow from the outer pockets, and since the constant orifices connecting the pockets and the displacement chambers are independent of the gap height, the inlet flow to the pockets allows the pocket pressure to reach a level similar to that of the displacement chamber, which provides additional force to counteract the cylinder block's moment imbalance. Conversely, when less force

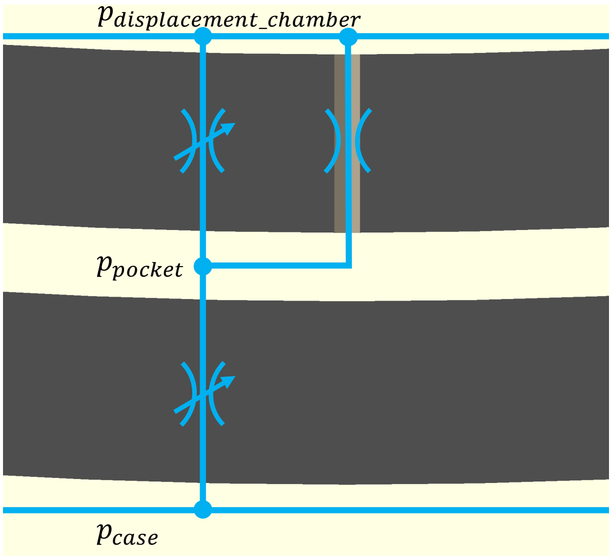

Figure 5: Hydraulic Circuit of Hydrostatic Pocket

is needed, a higher gap height increases the variable orifices' area, balancing the inlet and outlet flow to the pocket and reducing the hydrostatic pressure.

3 Modeling Approach

The modeling approach for simulating the cylinder-block/valve-plate lubricating interface was developed using a multi-physics simulation suite, Multics [12]. Although Multics is capable of simulating all three lubricating interfaces in a piston machine, as well as the dynamic coupling between each module, this study is limited to the cylinder-block/valve-plate interface, and the information flow is shown in Figure 6 [11].

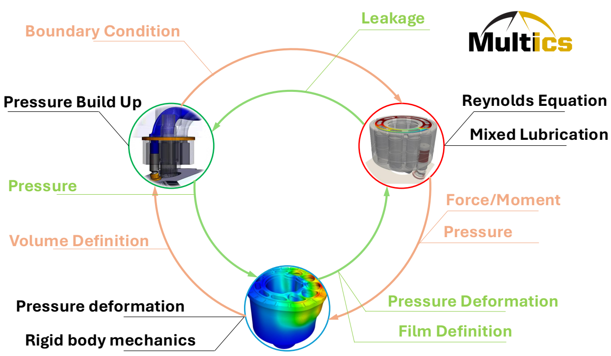

Figure 6: Modeling Information Flow

3.1 Lumped Parameter Model

The pressure within the displacement chambers is simulated using Hopsan [13], which employs a lumped parameter model as shown in Figure 7. The model computes the translational movements of the pistons and solves the continuity equation for each chamber. Pseudo-cavitation and the pressure dependency of the bulk modulus are considered. The openings of the chambers to each port are modeled as variable orifices. The model assumes no leakage and friction. The lumped parameter model is used to compute the pressure profile under consideration of commutation effects for each operating point. Multics then reads in the pressure profile in the displacement chambers as a look-up table based on the shaft rotation angle.

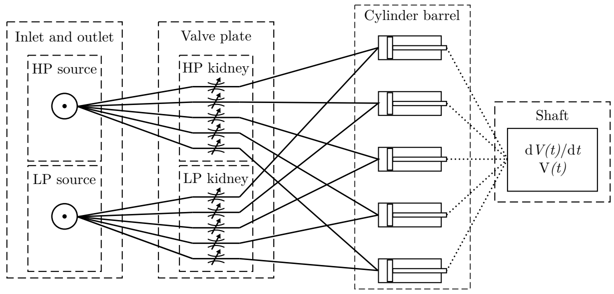

Figure 7: Lumped Parameter Model Structure. [14]

The pressure from the displacement chambers, used as the upstream pressure for the hydrostatic pockets, always connects to the pockets through constant-area orifices, which the area is determined for optimal power efficiency based on Achten et al.'s experimental results [2]. The mass flow rate through the orifices into a given hydrostatic pocket, $\dot{m}$, is calculated using the orifice equation shown in Eq. 2.

$$\dot{m} = C_d A \sqrt{2\rho \Delta p} \tag{2}$$

The hydrostatic pockets are modeled as fluid volumes, and the pressure is calculated using the isothermal pressure build-up equation, as shown in Eq. 3. Since there is no volume derivative for the hydrostatic pockets, the last term can be omitted.

$$\frac{\partial p}{\partial t} = \frac{K}{V}\left(\frac{1}{\rho}\dot{m}_{in} - \frac{1}{\rho}\dot{m}_{out} - \frac{\partial V}{\partial t}\right) \tag{3}$$

The pressures from the inlet ports, outlet ports, casing, displacement chambers, and hydrostatic pockets serve as pressure boundaries for the lubricating interface model. These pressures are also used to apply loads to the cylinder block.

3.2 Lubricating Film Model

There are three lubricating interfaces in a Floating Piston machine. However, since the focus of this study is on the effect of hydrostatic pockets on the cylinder block, and the majority of forces from the piston and piston plate do not transfer to the cylinder block, only the cylinder-block/valve-plate lubricating interface is simulated.

The traditional form of the Reynolds equation is written in terms of the pressure, as shown by Hamrock et al. [15]. However, this formulation is unable to simulate the cavitated regions in the lubricating interface precisely, leading to an incorrect flow estimation. Therefore, Ransegnola proposed the density-based Reynolds equation accounting for cavitation effects and providing accurate flow predictions [12]. In addition, Ransegnola utilized statistical mixed lubrication relations to formulate the universal mixed Reynolds equation, as shown in Eq. 4, which is used in Multics [16–18].

$$\nabla \cdot \left(\phi_p \frac{Kh^3}{12\mu} \nabla \rho \right) = \nabla \cdot (\rho \boldsymbol{v}_m (\phi_R R_q + \phi_c h)) \\ + \nabla \cdot \left(\rho \frac{\phi_s}{2} R_q (\boldsymbol{v}_t - \boldsymbol{v}_b) \right) + \frac{\partial \rho (\phi_R R_q + \phi_c h)}{\partial t} \tag{4}$$

The Reynolds equation predicts the pressure distribution within the lubricating interface and is critical for assessing power loss. The power loss considered in this study arises from the energy dissipation due to the viscous shear of the lubricating fluid with the consideration of the shear loss from high-pressure fluid leakage [19]. Viscous dissipation is a major contributor to power loss at the lubricating interface and is ultimately converted into heat. The governing equation for viscous dissipation in polar coordinates, as used in Multics, is presented below in Eq. 5 and Eq. 6.

$$P_{\text{loss}} = \iint \mu \phi_D \, dz \, dA \tag{5}$$

$$\phi_D = \left(\frac{\partial u}{\partial z} \right)^2 + \left(\frac{\partial v}{\partial z} \right)^2 + \frac{1}{r^2} \left(\frac{4}{3} u^2 + v^2 \right) \tag{6}$$

More importantly, for this study, the pressure distribution can be used to predict the volumetric leakage through the interface, which is crucial for simulating the correct behavior of the hydrostatic pockets. This is because the equivalent variable orifices connecting the hydrostatic pockets to the displacement chamber and casing are determined by the volumetric flow in the lubricating interface.

Additionally, Multics considers both penetration contact and asperity contact. Specifically, the asperity contact arises from the interaction of surface micro-structures due to roughness. Multics calculates the equivalent roughness between surfaces, incorporates material properties, and uses these to generate an asperity contact curve, from which the asperity contact pressure is determined based on the gap height [20].

Lastly, the combined pressure distribution from the lubricating interface and contact model is used for body dynamics calculations as well as solid-body deformation analysis to estimate the accurate gap height in the lubricating interface.

3.3 Body Dynamics Model

The axial forces and moments arising from the pressurized fluid in the displacement chambers and the lubricating interface are used to solve the equations of conservation of linear and angular momentum for the cylinder block body, as shown in Eq. (7) and Eq. (8); encompassing three degrees of freedom, allowing the cylinder block to move in the axial direction and tilt around the cylinder-block/shaft reaction point, or the crowing point, which also balances the block's radial forces and provides the drive torque to rotate the cylinder block [9].

$$m \frac{d\boldsymbol{v}_{IF}}{dt} = \sum \boldsymbol{F}_{l,IF} \tag{7}$$

$$[I_{BF}] \frac{d\omega_{BF}}{dt} = \sum \boldsymbol{M}_{l,BF} \tag{8}$$

The radial forces and moments from the wedge-shaped fluid inside the displacement chamber shown in Figure 8, caused by the tilted piston and piston sealing ring, are calculated using Eq. 9 and Eq. 10 [3].

$$F_{R,i} = \pi R_c^2 \tan \alpha \, p_{c,i} \tag{9}$$

$$F_{R,\text{tot}} = \sum_{i=1}^{z} F_{R,i} \tag{10}$$

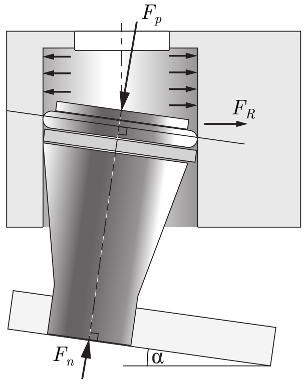

Figure 8: The Radial Force F_R [3]

Moreover, to accurately evaluate contact severity and power loss within the lubricating interfaces, it is essential to account for solid-body deformation [6]. In this simulation model, the half-space method based on the Hertzian contact stress is employed to evaluate the deformation in the cylinder block and valve plate caused by local fluid film pressure and contact pressure. Finally, the resulting cylinder block positions, velocities, and deformation are fed back to assess the influence of squeeze and wedge phenomena on the lubricating interface through the Reynolds equation.

4 Results and Discussion

4.1 Simulation Setup

Four groups of operating conditions are tested, as outlined in Table 1: Low-Speed High-Pressure (LSHP), High-Speed Low-Pressure (HSLP), High-Speed High-Pressure (HSHP), and Medium-Speed Medium-Pressure (MSMP). These conditions are defined by the rotational speed and outlet pressure, where low-speed is 300 rpm, medium-speed is 2000 rpm, and high-speed is 6000 rpm, while low-pressure is 20 bar, medium-pressure is 200 bar, and high-pressure is 350 bar.

To evaluate the effectiveness of the hydrostatic pockets, a baseline pump without pockets is simulated alongside configurations where pockets are positioned on the inside (Inner Pockets), outside (Outer Pockets), or both sides (Both Pockets) of the sealing land. Each configuration is further analyzed based on the pocket placement relative to the displacement chamber: one set positioned closer to the chamber (Small

Table 1: Simulated Pocket Designs and Operating Conditions.

Operating Condition	Baseline	Small Area Inner Pockets	Small Area Outer Pockets	Small Area Both Pockets	Large Area Inner Pockets	Large Area Outer Pockets	Large Area Both Pockets
Low-Speed High-Pressure	✓	✓	✓	✓	✓	✓	✓
High-Speed Low-Pressure	✓	✓	✓	✓	✓	✓	✓
High-Speed High-Pressure	✓	✓	✓	✓	✓	✓	✓
Medium-Speed Medium-Pressure	✓	✓	✓	✓	✓	✓	✓

Area) and the other set positioned farther away (Large Area) representing the different areas of the sealing land trapped between the pockets and the displacement chambers, as illustrated in Figure 9.

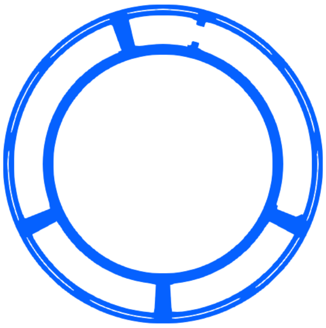

(a) Small Area - Outer Pockets

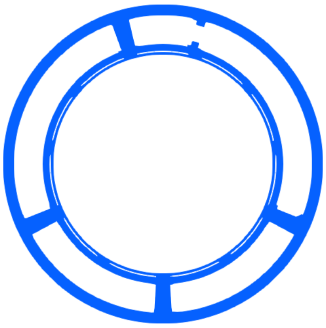

(b) Small Area - Inner Pockets

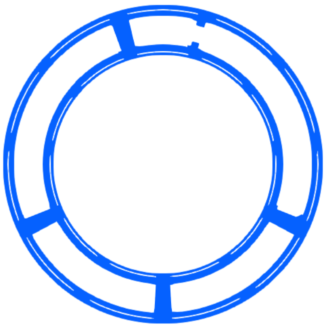

(c) Small Area - Both Pockets

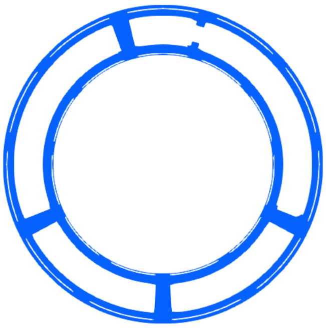

(d) Large Area - Both Pockets

Figure 9: Hydrostatic Pockets Location Examples

To create a fair comparison between the outer and inner pockets, the locations are determined by maintaining the lubricating interface area between the hydrostatic pockets and the displacement chambers. This assumption is based on the premise that the additional hydrostatic pressure in the lubricating film generated by the pockets is directly proportional to this area. Lastly, to accurately evaluate the efficacy of the hydrostatic pockets as well as the differences between different configurations, local meshing surrounding the pockets in the lubricating film model is refined.

To ensure the applicability of this study, a sensitivity analysis is performed under the medium-speed medium-pressure operating condition to determine the crowning point location for the remaining simulations. As introduced in the modeling approach section 3.3, the crowning point directly influences the moments applied to the cylinder block, impacting its stability and overall performance. As shown in Figure 10, the viscous power loss and the moments acting on the cylinder block are normalized for ease of comparison.

The green zone in the sensitivity analysis represents the optimal scenario, indicating that solid-body deformation, manufacturing tolerances, wear, and other factors are functioning without causing a large shift at the moments applied to the cylinder block. Meanwhile, the orange zone shows the scenarios where small disturbances may introduce some deviations, such as manufacturing imperfections and wear, but are still within acceptable limits. Finally, the red zone represents the extreme conditions where the cylinder block experiences significant moment imbalance, resulting in instability and further decreased performance. It can be seen that as the moment applied on the cylinder block increases, the viscous power loss for the baseline machine increases exponentially; meanwhile, with the addition of the hydrostatic pockets, the power losses are kept at a constantly low level.

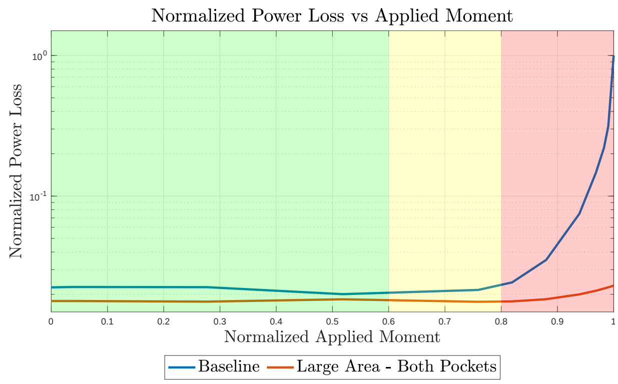

Figure 10: Normalized Power Loss vs. Applied Moment

For this study, simulations were conducted assuming a non-ideal crowning point for several reasons. First, testing the hydrostatic pockets under such conditions ensures this feature will remain effective even in the most non-optimal situations. Second, since the piston-seal/cylinder-bore friction forces and oil inertia forces are not included in these simulations, assuming a non-ideal crowning point would help to increase the robustness of this study. Lastly, while the baseline cylinder block in a Floating Piston pump exhibits mostly balanced moments, the study is made more general when the crowning point is placed sub-optimally due to the complexities of a typical axial piston unit, providing more reliable insights that can be applied to a wider range of applications.

4.2 Low-Speed High-Pressure Operating Condition

As discussed in Section 2.2.2, low-speed operating conditions are a major challenge for the cylinder-block/valve-plate lubricating interface in a piston machine due to the lack of the hydrodynamic wedge effect. Furthermore, the high outlet pressure presents a greater moment imbalance for the cylinder block caused by radial chamber forces. Thus, at this operating condition, the benefits from the addition of hydrostatic pockets become more pronounced. The lowest simulated speed performed is 100 rpm, and the results show similar behavior to the 300 rpm case discussed in this section; however, due to the nature of the simulation, decreasing shaft speed significantly increases wall time.

The maximum gap height of the cylinder-block/valve-plate lubricating interface is shown in Figure 11, while the minimum gap height is shown in Figure 12 over one displacement chamber period, which is 360 degrees divided by the number of pistons. The baseline case results show that the maximum gap height is close to 90 micrometers, while the minimum gap height is below 0.2 micrometers, indicating that the block is severely tilted. With the addition of hydrostatic pockets, not only does the minimum gap height increase and the maximum gap height decrease, but the cylinder block also exhibits a much lower amplitude of tilting oscillation, indicating that the unbalancing motion is significantly reduced.

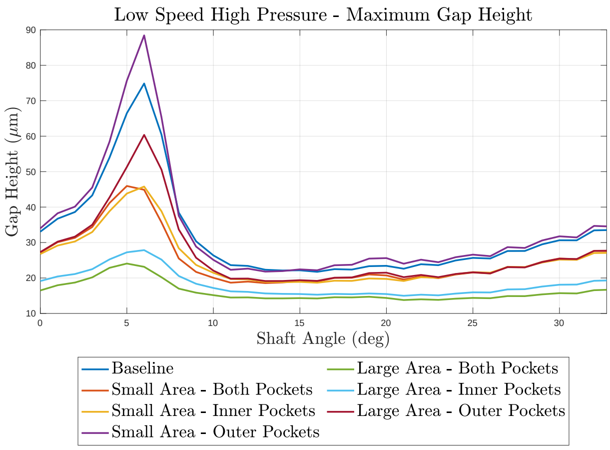

Figure 11: LSHP - Maximum Gap Height, h_{max}

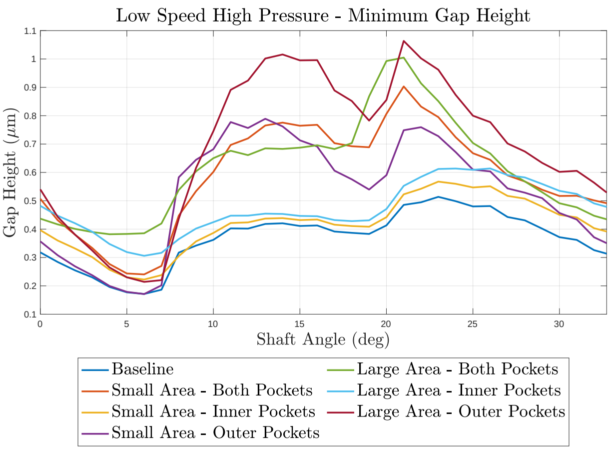

Figure 12: LSHP - Minimum Gap Height, h_{min}

The relief of strong tilting motion is also reflected in the metal-to-metal contact behavior. As shown in Figure 13, the baseline case experiences the highest magnitude of contact pressure, indicating that the lubricating film is unable to balance the moment. It is worth noting that in both the Large Area - Inner Pockets and Large Area - Both Pockets cases, no solid-body contact is observed.

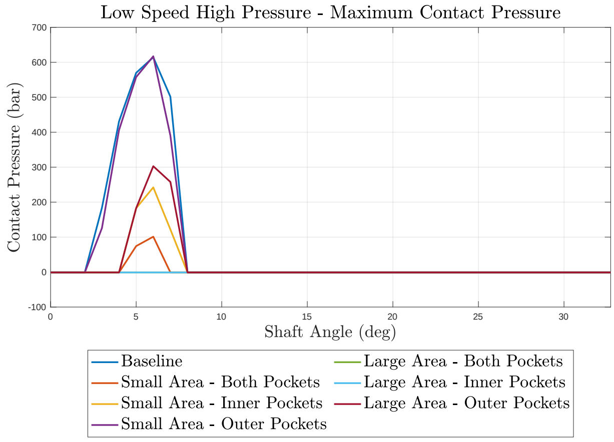

Figure 13: LSHP - Maximum Contact Pressure, p_{cont}

The condition in which the hydrostatic pockets are pressurized is an important aspect of this study. Figure 14 demonstrates that, initially, when the local gap height is large, the pressure in the outer pocket is maintained at approximately the average level between the casing and displacement chamber; and as the pocket transitions into the low gap height region, its pressure increases and approaches the level of the displacement chamber. For the inner pockets, as illustrated in Figure 15, the relatively neutral and stable gap height distribution towards the center of the cylinder block prevents a significant pressure increase. This distinction between inner and outer pockets showcases the dynamic behavior of pressurization in the hydrostatic pockets and their dependency on local film thicknesses.

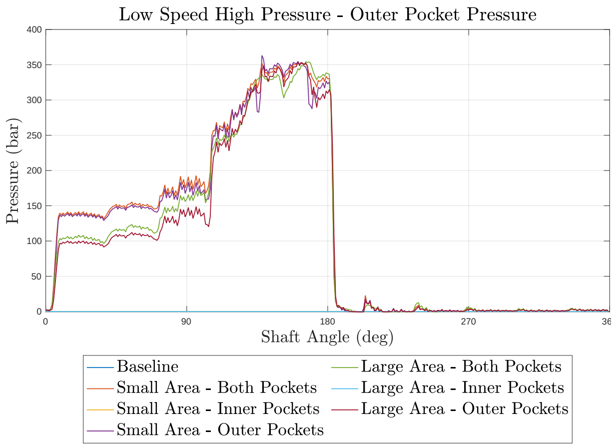

Figure 14: LSHP - Outer Pocket Pressure, p_{out}

This behavior can be further observed through the pressure distribution shown in Figure 16, where the colors represent pressure levels, with red being high pressure and blue being low pressure. The high-pressure delivery ports are located on the left side of the valve plate, and the cylinder block is rotating counterclockwise, as indicated in the figures. During the

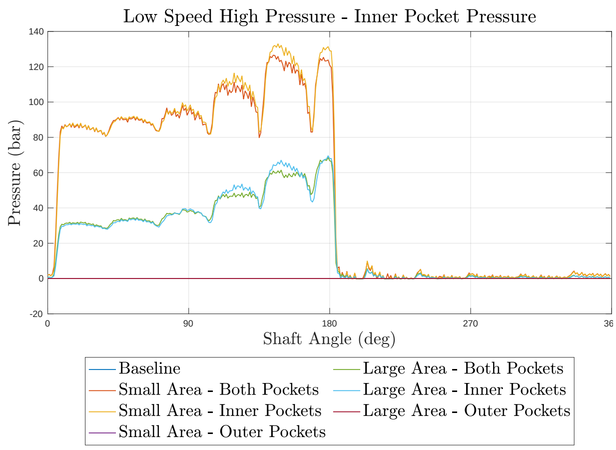

Figure 15: LSHP - Inner Pocket Pressure, p_{in}

high-pressure zone, as the displacement chamber rotates from the high gap height region to the low gap height region, the hydrostatic pocket begins to pressurize as its color approaches the color of the displacement chamber. This dynamic behavior demonstrates that hydrostatic pockets adapt their pressure and provide hydrostatic support depending on the gap height, passively mitigating tilting.

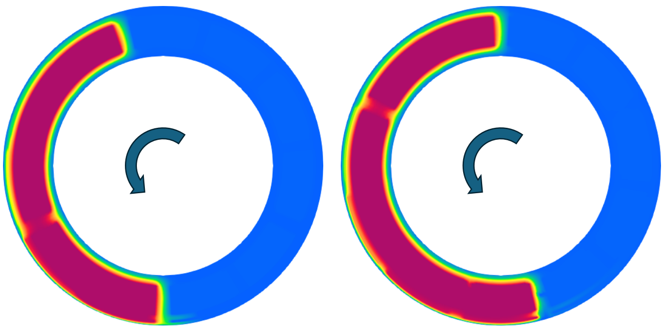

(a) 0 Deg *(b) 16 Deg*

Figure 16: LSHP - Large Area - Both Pockets - Film Pressure

Moreover, as shown in Table 2, the viscous power loss from the cylinder-block/valve-plate lubricating interface is reduced with the addition of the hydrostatic pockets, with the greatest reductions being the cases with the Large Area - Inner Pockets and Large Area - Both Pockets configurations. There are two key findings from the results. First, hydrostatic pockets not only generate additional hydrostatic force within their areas but also help elevate the pressure in the surrounding lubricating film, particularly when the gap heights are low, creating an additional boundary for the lubrication fluid between the pockets and displacement chambers. As shown in Figure 17, the pressure in the pockets and the fluid film approach similar levels as the displacement chamber. Therefore, locating the hydrostatic pockets farther away from the displacement chambers further increases the hydrostatic force when necessary, improving cylinder block balance.

The second point may seem counterintuitive. Although locating the pockets closer to the outer edge of the cylinder block sealing land generates larger balancing moments, the squeeze

Table 2: LSHP - Viscous Power Loss

Pocket Setup	Power Loss Reduction [%]
Baseline	-
Small Area - Inner Pockets	57.1
Small Area - Outer Pockets	-26.6
Small Area - Both Pockets	53.9
Large Area - Inner Pockets	82.5
Large Area - Outer Pockets	41.7
Large Area - Both Pockets	85.4

effect of the bearing results in high pressure near the outer edge, where gap heights are minimal and oscillating. This generated hydrodynamic pressure diminishes the contribution of the hydrostatic pockets, reducing their effectiveness. In contrast, positioning the pockets on the inner side of the sealing land, while having a shorter moment arm, enhances the pressure in the lubricating interface where all hydrodynamic effects are weak. Therefore, locating the hydrostatic pockets on the inner side of the cylinder block is more effective for mitigating block tilting and solid-body contact.

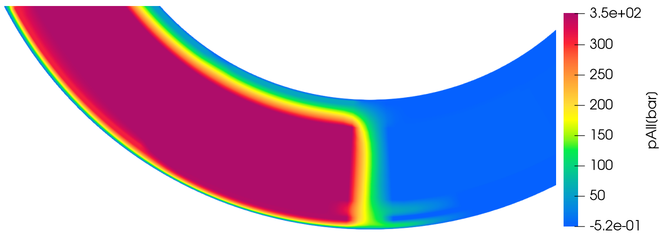

Figure 17: LSHP - Large Area - Both Pockets - Film Pressure Zoomed at 0 Deg

4.3 High-Speed High-Pressure Operating Condition

High-speed high-pressure condition also leads to challenges in lubricating the cylinder-block/valve-plate interface. While elevated rotational speeds enhance hydrodynamic wedge effects, helping balance the cylinder block and reduce viscous and contact losses, the simultaneous presence of high pressures increases the risk of moment imbalances, potentially compromising stability.

Simulation results in Figure 18 show that, under HSHP conditions, the baseline configuration exhibits large film thickness variation, causing increased tilting. The introduction of hydrostatic pockets improves the cylinder block stability by providing additional pressure support to counteract these tilting moments.

More specifically, Figure 19 illustrates how pocket pressure dynamically adjusts to film height variations in order to maintain more uniform gap height distributions and enhance moment balancing.

Table 3 compares viscous power losses across different hydrostatic pocket configurations, consistent with the low-speed high-pressure operating condition, showing that the Large

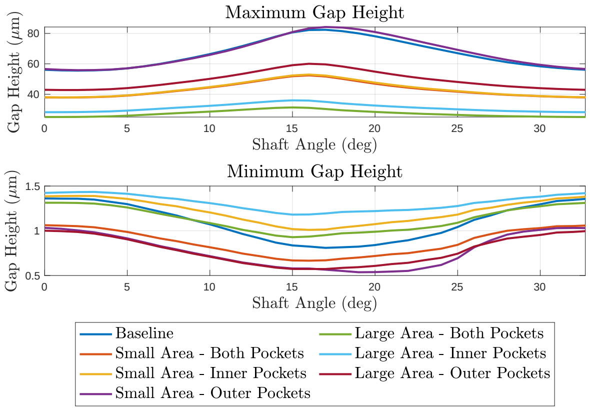

Figure 18: HSHP - Gap Heights, h_{max}, h_{min}

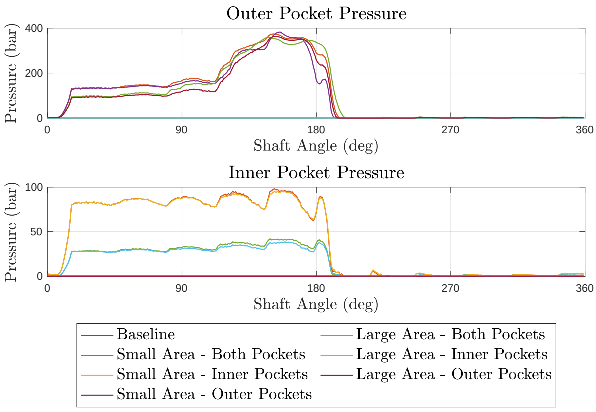

Figure 19: HSHP - Pocket Pressures, p_{out}, p_{in}

Area - Inner Pockets and Large Area - Both Pockets cases achieve the greatest reductions. These results further emphasize the importance of the hydrostatic pocket placements to maximize performance.

Table 3: HSHP - Viscous Power Loss

Pocket Setup	Power Loss Reduction [%]
Baseline	-
Small Area - Inner Pockets	59.8
Small Area - Outer Pockets	-4.5
Small Area - Both Pockets	60.9
Large Area - Inner Pockets	73.3
Large Area - Outer Pockets	50.7
Large Area - Both Pockets	76.6

4.4 High-Speed Low-Pressure Operating Condition

Compared with the LSHP and HSHP operating conditions, the high-speed low-pressure case is inherently more stable due to the strong hydrodynamic edge effects resulted by high relative sliding velocity and low radial chamber forces and moments, as shown in Figure 20.

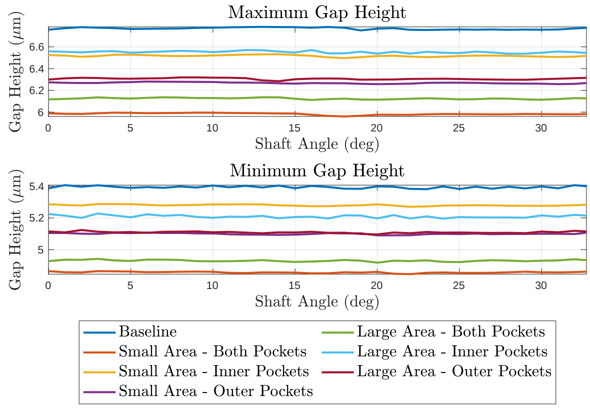

Figure 20: HSLP - Gap Heights, h_{max}, h_{min}

The pressure within the hydrostatic pockets does not increase significantly as shown in Figure 21, indicating that the hydrostatic pockets are not over-pressurized when there is no motivation to create additional balancing moments on the cylinder block.

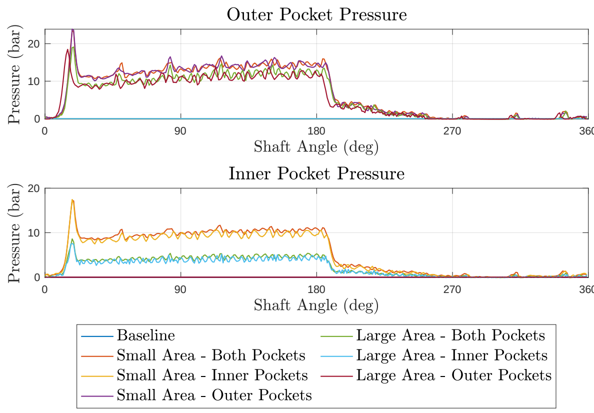

Figure 21: HSLP - Pocket Pressures, p_{out}, p_{in}

Lastly, since there is no excessive moment tilting the cylinder block, the power loss reduction due to the hydrostatic pockets is less significant. However, the slight reduction, as shown in Table 4 suggests that hydrostatic pockets can still provide benefits even when the cylinder block is inherently balanced.

Table 4: HSLP - Viscous Power Loss

Pocket Setup	Power Loss Reduction [%]
Baseline	-
Small Area - Inner Pockets	0.42
Small Area - Outer Pockets	2.82
Small Area - Both Pockets	1.92
Large Area - Inner Pockets	-0.01
Large Area - Outer Pockets	3.44
Large Area - Both Pockets	3.96

4.5 Medium-Speed Medium-Pressure Operating Condition

Unlike some other operating conditions examined, the medium-speed medium-pressure operation conditions do not typically lead to severe failure of the pump, such as strong metal-to-metal contact or excessive gap height variation; however, since hydraulic machines frequently operate under these conditions, the power efficiency is critical. Table 5 presents the power loss reduction with and without the incorporation of hydrostatic pockets, and the results are aligned with the findings under other operating conditions.

Table 5: MSMP - Viscous Power Loss

Pocket Setup	Power Loss Reduction [%]
Baseline	-
Small Area - Inner Pockets	90.7
Small Area - Outer Pockets	59.1
Small Area - Both Pockets	90.8
Large Area - Inner Pockets	95.1
Large Area - Outer Pockets	90.3
Large Area - Both Pockets	95.9

5 Discussion

A summary of the result comparison between the baseline design and the Large Area - Both Pockets case is presented in Figures 22 and 23. The figures show the largest values of maximum gap height and the smallest values of minimum gap height over one revolution, respectively. The data suggest that across various operating conditions, the maximum gap heights for the Large Area - Both Pockets case are consistently lower than those for the baseline case. Conversely, the minimum gap heights for the Large Area - Both Pockets case are either similar to or higher than those of the baseline case, which effectively prevents solid contact.

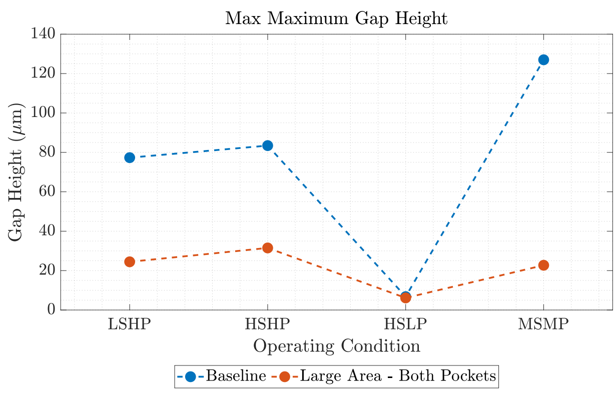

Figure 22: Maximum h_{max}

This study's findings align with Achten et al.'s experimental work on Floating Cup pumps with hydrostatic pocket integration, demonstrating that the addition of hydrostatic pockets can create a more uniform film thickness, reduce viscous power loss, enhance cylinder block stability, and mitigate substantial solid-body contact on the sealing land [2]. This paper examined multiple hydrostatic pocket configurations in addition to Achten et al.'s study, confirming that the pressure distribution in the lubricating interfaces and the pressure in the pockets shows that the hydrostatic pockets provide a dynamic and passive stabilizing effect to the cylinder block.

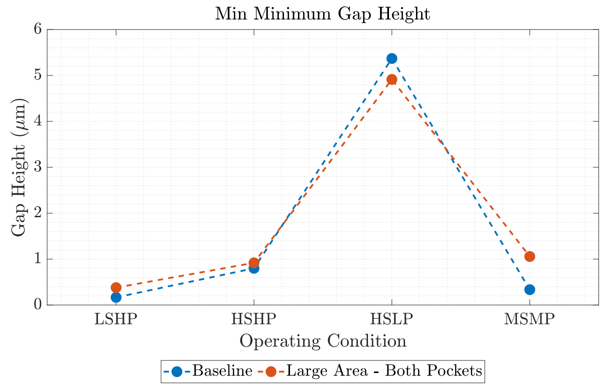

Figure 23: Minimum h_{min}

The placement of hydrostatic pockets is a critical design consideration. Although it may seem intuitive that positioning pockets toward the outer edge would generate larger balancing moments, our results suggest that the squeeze and wedge effects in the low gap height region already generate sufficient pressure, diminishing the pockets' influence. Instead, placing the hydrostatic pockets on the inside of the displacement chambers can supplement lubrication where hydrodynamic effects are the weakest. This finding is consistent across all four operating conditions simulated, and interestingly, in Achten et al.'s experimental study, only inner hydrostatic pockets were employed [2]. When the hydrostatic pockets are positioned farther from the displacement chamber, namely, the Large Area - Inner Pockets and Large Area - Both Pockets cases, the highest reductions in power losses are yielded (Table 3). Furthermore, since the Large Area - Inner Pockets and Large Area - Both Pockets configurations exhibit similar performance in all aspects, the Large Area - Inner Pockets setup alone would be sufficient when considering manufacturing cost-effectiveness.

6 Conclusion

This study showcases the effectiveness of hydrostatic pockets by improving the lubrication performance of piston-type machines, supporting and extending Achten et al.'s [2] experimental findings. Using advanced computational modeling techniques, the impact of the hydrostatic pockets is analyzed under several operating conditions, which resulted in improved gap height uniformity, pressure distribution, contact behavior, and overall efficiency; more generally, the addition of hydrostatic pockets would allow piston-type machines to broaden their range of operating speeds.

Out of all the setups simulated, placing the hydrostatic pockets on the inside of the cylinder block sealing land and farther away from the displacement chambers achieved the best performance in maintaining gap height, preventing metal-to-metal contact, and reducing power loss. The results demonstrate the importance of the placement of the hydrostatic pockets for lubrication performance and provide guidance for designing future piston-type machines.

However, the study also has limitations. Future research will refine the simulation model by including different hydrostatic pocket sizes, piston-seal/cylinder-bore lubricating interface, as well as the influence matrix and thermal deformation to further improve prediction accuracy. Experimental tests on the Floating Piston pump, incorporating hydrostatic pockets are intended to focus on evaluating efficiency across various shaft speeds. Additionally, torque losses at low speeds will be computed to validate the separation of the surfaces, and volumetric losses will be analyzed as they can can correlate with gap heights. Furthermore, a visual inspection of component surface wear will be carried out.

Acknowledgement

Linköping University's contribution was funded by the Swedish Electromobility Centre with grant number 13070 and the Swedish Energy Agency (Energimyndigheten) with grant number P2023-00594. The share of simulations run at Linköping University were enabled by resources provided by the National Supercomputer Centre (NSC), funded by Linköping University.

Nomenclature

Designation	Denotation	Unit
$\boldsymbol{A}$	Orifice area	[m^2]
α	Tilt angle of the piston plate	[rad]
$\boldsymbol{C}_d$	Discharge coefficient	[-]
$\eta_{\text{tot,p}}$	Total power efficiency loss	[-]
$\boldsymbol{F}_{\text{comp}}$	Hydrostatic compensation force	[N]
$\boldsymbol{F}_{\text{load}}$	Load force on the cylinder block	[N]
$\boldsymbol{F}_{l,\text{IF}}$	Sum of forces in inertia frame	[N]
$\boldsymbol{F}_R$	Radial force due to wedge-shaped fluid in displacement chamber	[N]
$\boldsymbol{h}$	Lubricating film thickness	[m]
$\boldsymbol{I}_{\text{BF}}$	Inertia tensor of the block frame	[kg·m^2]
$\boldsymbol{K}$	Bulk modulus	[Pa]
$\boldsymbol{M}_{l,\text{BF}}$	Sum of moments acting on the block frame	[N·m]
$\boldsymbol{m}$	Mass of the cylinder block	[kg]
$\dot{\boldsymbol{m}}$	Mass flow rate	[kg/s]
μ	Dynamic viscosity	[Pa·s]
ω_{BF}	Angular velocity of the block frame	[rad/s]
$\boldsymbol{p}$	Pressure	[Pa]
$\boldsymbol{p}_{\text{in}}$	Inlet pressures	[Pa]
$\boldsymbol{p}_{\text{out}}$	Outlet pressures	[Pa]
$\boldsymbol{P}_{\text{loss}}$	Viscous power loss	[W]
$\Delta\boldsymbol{p}$	Pressure difference across the orifice	[Pa]
$\phi_p, \phi_R, \phi_c, \phi_s$	Mixed lubrication flow factors	[-]
ϕ_D	Dissipation function	[-]
$\boldsymbol{r}$	Radial coordinate in polar form	[m]
$\boldsymbol{R}_c$	Radius of the sealing ring	[m]
$\boldsymbol{R}_q$	Surface roughness parameter	[μm]
ρ	Fluid density	[kg/m^3]
$\boldsymbol{t}$	Time	[s]
$\boldsymbol{u}, \boldsymbol{v}$	Velocity components in the interface	[m/s]
$\boldsymbol{V}$	Volume of hydrostatic pocket	[m^3]
$\boldsymbol{V}_d$	Displacement volume	[m^3]
$\boldsymbol{v}_{\text{IF}}$	Velocity of the inertia frame	[m/s]
$\boldsymbol{v}_m$	Mean velocity of the fluid in the interface	[m/s]
$\boldsymbol{v}_t, \boldsymbol{v}_b$	Surface velocities of the top and bottom plates	[m/s]
ζ	Hydrostatic compensation ratio	[-]
LSHP	Low speed high pressure	
HSLP	High speed low pressure	
HSHP	High speed high pressure	
MSMP	Medium speed medium pressure	

References

[1] J. Ivantysyn and M. Ivantysynova. *Hydrostatic Pumps and Motors, Principles, Designs, Performance, Modeling, Analysis, Control and Testing*. Academia Books International, New Delhi, India, 2001.

[2] P. Achten, R. Mommers, J. Potma, and J. Achten. Experimental investigation of a hydrostatic bearing between barrels and port plates in floating cup axial piston pumps. In *BATH/ASME 2020 Symposium on Fluid Power and Motion Control*, 2020.

[3] Liselott Ericson and Jonas Forssell. A Novel Axial Piston Pump/Motor Principle With Floating Pistons: Design and Testing. In *BATH/ASME 2018 Symposium on Fluid Power and Motion Control, FPMC2018*. American Society of Mechanical Engineers, 2018.

[4] P. Achten and S. Eggenkamp. Barrel tipping in axial piston pumps and motors. In *Proceedings of the 14th International Fluid Power Conference*, volume 144, pages 381–391, 2017.

[5] M. Ernst and A. Vacca. Hydrostatic vs. hydrodynamic components of fluid pressure in the tribological interfaces of axial piston machines. *Tribology International*, 157:106878, 2021.

[6] R. Chacon and M. Ivantysynova. An investigation of the impact of the elastic deformation of the endcase/housing on axial piston machines cylinder block/valve plate lubricating interface. In *Proceedings of the 10th IFK International Conference on Fluid Power*, volume 1, pages 283–294, Dresden, Germany, 2016.

[7] P. A. J. Achten, T. L. v. d. Brink, and G. E. M. Vael. A robust hydrostatic thrust bearing for hydrostatic machines. In *Proc. 7th International Fluid Power Confer-*

ence (IFK), pages 100–112, Aachen, Germany, March 22–24 2010.

[8] Stephan Wegner, Stefan Gels, and Hubertus Murrenhoff. Vergleich analytischer Berechnungsmethoden des Entlastungsgrades im Kolbentrommel-Steuerspiegel-Kontakt in Axialkolbenmaschinen. *O+P Fluidtechnik*, 11-12/2017:60–69, 2017.

[9] N. D. Manring. Tipping the cylinder block of an axial-piston swash-plate type hydrostatic machine. *Transactions of the ASME*, 122:216–221, 2000.

[10] Andrea Vacca and Germano Franzoni. *Hydraulic Fluid Power: Fundamentals, Applications, and Circuit Design*. John Wileys and Sons, 2021.

[11] M. Zecchi and M. Ivantysynova. A novel approach to predict the cylinder block/valve plate interface performance in swash plate type axial piston machines. In *Bath/ASME Symposium on Fluid Power and Motion Control*, Bath, UK, 2012.

[12] T. Ransegnola. *A strongly coupled simulation model of positive displacement machines for design and optimization*. PhD Dissertation, Purdue University, West Lafayette, Indiana, 2020.

[13] Linköping University (Division of Fluid and Mechatronic Systems). Hopsan. https://liu.se/en/research/hopsan, accessed 2025-02-17.

[14] Thomas Heeger. *Design of Electro-Hydraulic Energy Converters : With Focus on Integrated Designs and Valve Plate Rotation*, volume 1971 of *Linköping Studies in Science and Technology. Licentiate Thesis*. Linköping University Electronic Press, Linköping, jun 2023.

[15] B. J. Hamrock, B. J. Schmid, and B. O. Jacobson. *Fundamentals of Fluid Film Lubrication*. CRC Press, 2004.

[16] N. Patir and H. S. Cheng. An average flow model for determining effects of three-dimensional roughness on partial hydrodynamic lubrication. *J. Lubr. Technol.*, 100(1):12–17, 1978.

[17] N. Patir and H. S. Cheng. Application of average flow model to lubrication between rough sliding surfaces. *J. Lubr. Technol.*, 101(2):220–229, 1979.

[18] C. Wu and L. Zheng. An average reynolds equation for partial film lubrication with a contact factor. *J. Tribol.*, 111(1):188–191, 1989.

[19] A. Schenk and M. Ivantysynova. An investigation of the impact of elastohydrodynamic deformation on power loss in the slipper swashplate interface. In *Proc. 8th JFPS International Symposium on Fluid Power*, Okinawa, Japan, 2011.

[20] Si C. Lee and Ning Ren. Behavior of elastic-plastic rough surface contacts as affected by surface topography, load, and material hardness. *Tribology Transactions*, 39(1):67–74, 1996.